Numerical Simulation of Seaplane Wave Ground Effect with Crosswind

*LI Yanghui, FU Xiaoqin, CHEN Jichang, TONG Mingbo**

National Defense Key Laboratory of Aircraft Advanced Design Technology, Nanjing University of Aeronautics and Astronautics, Nanjing 210016, P.R. China

(Received 25 April 2021; revised 10 June 2021; accepted 15 July 2021)

Abstract: Under the absolute coordinate system, the unsteady Reynolds averaged Navier-Stokes (URANS) equations and the k-ω SST turbulence model are solved using the finite volume method to simulate the aerodynamic characteristics of large seaplane flying with the ground-effect above wavy surface. The velocity inlet wave-making method and the volume of fluid model are used to accurately simulate the linear regular waves and to precisely capture the free surface. This paper studies the influence of the sideslip angle on the aerodynamic characteristics of large seaplane when it is cruising above wavy water. The results show that the wave surface mainly affects the pressure distribution on the lower surface of the wing. When the sideslip angle varies from 0° to 8°, the varying of frequency of aerodynamic forces is consistent with the wave encounter frequency, and both periods are 0.6 s. With the increase of the sideslip angle, the lift coefficient and the pitching moment coefficient decrease. However, when the sideslip angle is smaller than 4°, the decrease amplitude is small, and the significant decrease occurs above 4° and during the whole process of the change of sideslip angle, the aerodynamic fluctuation amplitude is almost unchanged. As the drag coefficient increases with the increase of sideslip angle, significant increase also occurs when the value is greater than 4°, and the fluctuation amplitude does not show any correlations. The rolling moment coefficient and yaw moment coefficient increase with the increase of the sideslip angle, and the fluctuation amplitudes of both increase linearly with the increase of the sideslip angle.

Key words: two-phase flow; wing-in-ground (WIG) effect; volume of fluid (VOF) model; velocity-inlet boundary wave maker

CLC number: V211.3 **Document code:** A **Article ID:** 1005-1120(2021)S-0001-09

0 Introduction

The wing-in-ground effect (WIG) is an aerodynamic effect that can reduce the induced drag of an aircraft and obtain a higher lift-to-drag ratio. When the aircraft is very close to the ground (water surface), the pressure difference between the upper and the lower wing surfaces will increase, resulting in a sudden increase in lift. In recent years, the development of amphibious aircraft in China has prompted the research demand for aerodynamic characteristics of aircraft in the ground-effect area. Compared with the ground, the water may be calm or wavy. The wave motion causes the change of the channel between the aircraft and the water surface, which makes the aerodynamic characteristics of the aircraft change. Especially in sideslip flight, the coupling of wave and ground effects makes the aerodynamic characteristics greatly different from those under calm water condition. Based on the above factors, both the shape of the water surface and the sideslip angle have an impact on the intensity of ground effect when the aircraft is cruising on the wave surface. Therefore, it is necessary and of certain engineering significance for the numerical simulation to be conducted on large seaplanes cruising on the wave surface.

The economic benefits of ground effect drive

*Corresponding author, E-mail adress: tongw@nuaa.edu.cn.

How to cite this article: LI Yanghui, FU Xiaoqin, CHEN Jichang, et al. Numerical simulation of seaplane wave ground effect with crosswind[J]. Transactions of Nanjing University of Aeronautics and Astronautics, 2021, 38(S): 1-9.

http://dx.doi.org/10.16356/j.1005-1120.2021.S.001

people to carry out further research on it. Early studies of ground effect mainly focused on wing and hard ground wave. Through wind tunnel tests, Jung et al.[1] analyzed the effects of aspect ratio, angle of attack, ground clearance and endplate on the aerodynamic characteristics such as lift and drag coefficients, pitching moment and aerodynamic center of NACA6409 airfoil through ground wind tunnel experiments, and visualized the near-ground flow field of NACA6409 airfoil through smoke trail tests. The results show that the vorticity at the wing tip decreases, the wake decreases, the lift increases, and the drag decreases. Ahmed et al.[2] simulated the hard ground with a conveyor system and carried out an experimental analysis of NACA4412 airfoil in a low-turbulence wind tunnel ($Re=3.0\times10^5$). The pressure distributions at different angles of attack and different ground clearances are analyzed. Ref.[3] used sliding-grid method to simulate the ground effect of a three-dimensional equal-straight wing NACA0015 flying over the high sea wave ground. The variation trend and reason of wing aerodynamic characteristics with flight altitude were analyzed. On this basis, the aerodynamic coefficients and roll moments of a straight wing under different sideslip angle were studied, and the aerodynamic characteristics of a straight wing under critical sea conditions were discussed. Ref.[4] numerically simulated the flow field of a ground-effect aircraft flying over a wavy ground using sliding mesh technology to study the influence of the aerodynamic performance of a wavy ground. It was concluded that the aerodynamic force is periodic when flying above the cosine wave ground, and the relationship between the flight altitude and angle of attack and the aerodynamic characteristics were analyzed. Most of the above researches on ground effect are limited to a single medium, and the wave surface can be obtained by changing the shape of the ground, which is different from the actual wave surface to some extent. Ref.[5] used volume of fluid(VOF) method to simulate the wave surface and carried out numerical simulation for NACA2410 airfoil flying over the wave surface, so as to obtain the flow field during flight. It was found that the influence of Wavy ground and wavy water on the aerodynamic characteristics of the airfoil was different. Meanwhile, the influence of wavy level on the ground effect of the airfoil was studied. By solving the incompressible unsteady Reynolds averaged Navier-Stokes equations, Ref.[6] numerically studied the ground effect of NACA4412 airfoil on wavy water surface, and compared the aerodynamic characteristics with those on flat rigid wall surface, static water and wavy rigid ground. The actual wavy surface has strong interaction with the airflow under the airfoil due to its own disturbance velocity, so the rigid wall surface cannot be used to study the wave ground effect. With the research field of real aircraft flying in ground effect area of water surface, Ref.[7] studied the aerodynamic characteristics of albatross when flying above the waves by using the plane element method. The results show that the flight efficiency of albatross depends not only on the speed and height of flight, but also on the amplitude and wavelength of flight. Ref.[8] carried out numerical simulation of lateral wind taking-off and landing based on the 1∶15 scaled model of AG600 seaplane, and analyzed the influence of propeller slip flow on yaw moment instability of lateral wind take-off and landing state through comparison with wind tunnel experimental.

In real flight, the seaplane is under coupling effect of wave ground effect and sideslip angle at the period of after taking off or before landing due to the wind and rough sea. However, from the research content of the above scholars, there has not been a complete numerical simulation process and analysis of large seaplane flying above wavy surface considering ground effect.

In this paper, the velocity inlet wave-making method combined with the VOF method is used to accurately capture the wavy surface. By using the finite volume method, the aerodynamic characteristics and flow field characteristics of aircraft flight in the wavy ground effect area are obtained. The difference of aerodynamic performance between sideslip flight and windward flight is compared, which can provide some reference for the practical cruising problem of seaplanes above wavy water.

1 Numerical Method

1.1 Fluid control method

The governing equations for the unsteady flow of the present study are unsteady incompressible Reynolds averaged Navier-Stokes (URANS) equations combined with the shear stress transport k-ω SST turbulence model. The finite volume method is used to discretize the governing equations in space, the second-order upwind scheme is selected for time discretization and the calculation process adopts the dual time step method.

1.2 Free surface treatment

Waves have a water-air interface that changes with time due to free surface flow. The essence of numerical wave generation is to numerically simulate the shape and position of the free surface that changes with time and the different fluid characteristics of the upper and lower regions of the free surface. Therefore, processing the free surface becomes the key to the numerical wave generation problem. In this paper, a simple and stable VOF method is used to track the shape and position of the free surface in real time. The principle is to determine the position and shape of the free surface by using the ratio function F between the change of the fluid volume in the cell and the volume of the cell. The variation range of F is 0—1. Judging F of each grid, when F=0.5, it means that this is a water-air interface, F=1 means that the grid is all water, and F=0 means that the cell is all air, as shown in Fig.1. For the air area above the water surface, the pressure is maintained at 101 325 Pa. In the water area below the water surface, the pressure $P=\rho gh$, and h is the water depth.

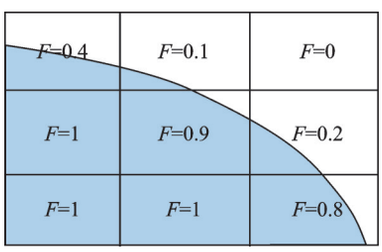

Fig.1 Schematic of VOF

1.3 Velocity-inlet boundary wave maker

Currently, the most used wave making methods mainly include rocking plate wave making method, source term wave making method and velocity-inlet wave making method. Considering the simplicity of setting and taking the accuracy of calculation into account, this paper adopts the velocity-inlet boundary wave making method to realize wave simulation. The wave position and the water quality points' velocity are applied to the entrance boundary and spreaded into the flow field as time progresses. For linear regular waves, the wave surface height changes periodically with the position coordinate x and time t, and the wave surface equation is

$$\eta(x,t)=\frac{H}{2}\cos(kx-\omega t) \tag{1}$$

where η is the wave surface height, H the wave height, x the coordinate of the water quality point, k the wave number, and ω the circular frequency. The expressions of the horizontal velocity component u and the vertical velocity component v of the water quality point (x, y) in the wave are written as

$$\begin{cases} u=\dfrac{\partial\varphi}{\partial x}=\dfrac{\pi H}{T}\cdot\dfrac{\cosh k(y+d)}{\sinh kd}\cos\theta_x \\ v=\dfrac{\partial\varphi}{\partial y}=\dfrac{\pi H}{T}\cdot\dfrac{\sinh k(y+d)}{\sinh kd}\sin\theta_x \end{cases} \tag{2}$$

where φ is the velocity potential function, T the period, d the water depth, and θ_x the angle between the wave propagation direction and the positive x-axis. The wave parameter description is shown in Fig.2.

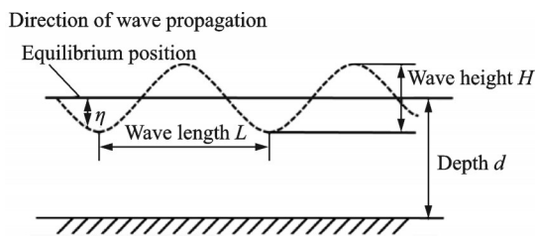

Fig.2 Wave parameters and different positions of waves

The accuracy validation of wave generation has been completed in Refs.[9-10], so it will not be repeated it in the paper.

2 Validation

At present, there are few domestic and foreign experimental studies on numerical simulation of two-phase flow wave ground effect. Ref.[3] studied the influence of calm water surface on the ground effect of the wing and found that the water surface deformation was very small, not enough to affect the aerodynamic force on the wing. Therefore, under calm water surface conditions, rigid walls can be used instead of real water surfaces to study wave ground effects.

This section is mainly based on the CFD method to perform numerical calculations of the flow around the NACA4412 airfoil flying over real calm water. The calculated results are compared with the test data of NACA4412 over rigid ground in Ref.[2].

2.1 Model and mesh

There is an experimental study on the ground effect of NACA4412 airfoil in in Ref.[2]. The experiment was carried out in a low turbulence wind tunnel at a speed of 30.8 m/s. The model is an isometric airfoil with a NACA4412 cross-sectional airfoil, and the wing chord length c is 150 mm. The extension is 600 mm. Both ends of the wing are equipped with end plates to reduce the three-dimensional effect and better show the aerodynamic characteristics of the airfoil. The experiment diagram is shown in Fig.3[2].

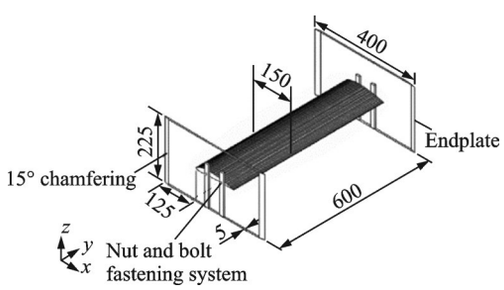

Fig.3 Schematic diagram of test model[2]

In numerical simulation, the left, right and top of the calculation domain are 15 times of the chord length, and the bottom is set to 1 m. Since the above experiment simulates the two-dimensional airfoil ground effect, the size of the flow field in the spanwise of the wing does not need to be consistent with the experiment. In this paper, only one layer of grids is set in the spanwise of the wing, with a length of 0.02 m. At the same time, the area near the water surface location is encrypted. The grid is divided, as shown in Fig.4. The minimum grid size is 0.000 01 m and the maximum is 0.02 m. The left, upper, and lower boundaries of the wing are the velocity inlet boundary conditions, the two boundary surfaces in the span of the wing are the symmetry boundary conditions, and the right boundary is the pressure outlet boundary conditions. The boundary conditions of the model are shown in Fig.4(a). The position of the water surface and the airfoil at the initial time are shown in Fig.4(b). In numerical simulation, the flying height h is defined as the vertical distance between the trailing edge of the airfoil and the ground. A total of three working conditions of h/c=0.15, 0.4 and 1 are calculated. Among them, the time step size is 0.001 s, and the total physical time is 1 s. Fig.5 gives the wave initial phase.

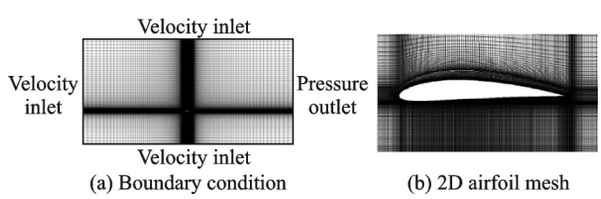

Fig.4 2D mesh and boundary condition

Fig.5 Wave initial phase

2.2 Results

Fig.6(a) shows the comparison chart of airfoil pressure coefficient C_p when h/c=0.15. It can be seen that the distribution trend of the calculated pressure coefficient is consistent with the experimental value. The pressure coefficient value obtained by the overall numerical simulation is slightly smaller than the experimental value, and the pressure coefficients at the leading edge and the trailing edge of the airfoil are in high agreement with the experimental values. Fig.6(b) shows the comparison chart of airfoil pressure coefficient when h/c=0.4. At this time, the pressure coefficient on the lower surface of the airfoil

is slightly larger than the experimental value, and the upper surface pressure coefficient is almost completely consistent with the experimental value. Fig.6(c) shows the comparison chart of airfoil pressure coefficient when $h/c=1$. At this time, the pressure coefficient on the lower surface of the airfoil is in good agreement with the experimental value, and the pressure coefficient obtained on the upper surface is slightly larger than the experimental value. To sum up, the values obtained by numerical simulation have the same change rule with the experimental values. Although the results have some errors, they are all within a reasonable range. Moreover, when h/c is too small, the value obtained by numerical simulation has a larger error from the experimental value, and the error will decrease with the increase of h/c.

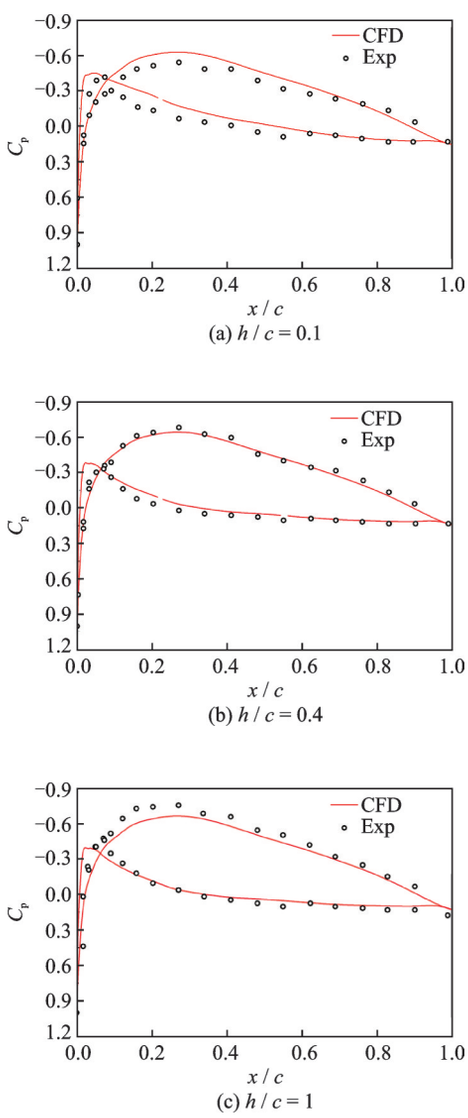

Fig.6 Comparison of pressure coefficient

3 Computational Setup

3.1 Seaplane model and flight conditions

The seaplane model is shown in Fig.7. The coordinate system is fixed on the aircraft, the origin of coordinates is located at the leading edge point of the nose, the x-axis is parallel to the flight direction and points downstream, and the z-axis is inside the plane of symmetry and points upwards. The mass of the seaplane is 49 t, the barycenter coordinate is (17, 0, 1.01), the 1/4 aerodynamic center position is 38%MAC, and the average aerodynamic chord length of the whole machine is 4.5 m. It has a wingspan of 36 m. The wing area is 167.235 m^2. The specific parameters of the model are shown in Table 1. The body is arranged with a single upper wing, and the bottom is a ship-type structure with a step.

(a) CAD model (b) Mesh

Fig.7 Schematic and mesh for the airplane

Table 1 Airplane parameters

Parameter	Value
Center of gravity / m	(17,0,1.01)
Half span / m	18
Body length / m	36
Mass / kg	4.9×10^4
Pitch moment of inertia	2.52×10^6

This paper mainly discusses the differences of aerodynamic characteristics of aircraft flying on wavy water surface under different sideslip angles, so it mainly involves the changes of aircraft flight altitude parameters, wave parameters and aircraft attitude. The flight altitude is defined as the vertical distance model between the aerodynamic center and the wave at the equilibrium position. Considering that h/c of the single wing on the plane layout is too small and the aircraft will contact the water, $h/c=1.5$ is taken in this paper. The calculation conditions and wave parameters are shown in Table 2.

Table 2 Flying parameters

Parameter	Value
Flight height h/c	1.5
Flying speed / ($m \cdot s^{-1}$)	70
Angle of attack / (°)	0
Sideslip angle / (°)	0, 2, 4, 6, 8
Wave length / m	45
Wave height / m	1.6

3.2 Mesh and boundary conditions

Based on the STAR CCM+ software, a hexahedron domain is constructed for this problem and the volume is split between air and water, as shown in Fig.8. The dimensions of the block are as follows: The x direction of the computational domain is 180 m, coordinate (−150 m, 50 m). y direction is 50 m, coordinate (−50 m, 50 m), and z direction is 55 m, coordinate (−25 m, 30 m). The aircraft is flying in the ground effect area, and the front and rear edges of the wing, as the main components to generate aerodynamic force, need additional encryption. The surface mesh is as shown in Fig.7(b). In order to achieve accurate wave capture, the area close to the surface equilibrium position needs to be additionally encrypted, that is, the height from the calculation area z to the surface equilibrium position ±1 m. When the wave propagates to the outlet boundary, there will be backflow, which will affect the flow field and calculation accuracy. Therefore, the sparse grid is separated from the pressure outlet boundary by 50 m to achieve the effect of physical wave elimination. At the same time, the air area under the aircraft wing and in the middle of the water surface is the ground effect area, which also needs to be encrypted separately. The surface layer of the body is 20 layers, the height of the first layer is 0.000 5 m, and the biggest size of the grid is 5 m. The volume grid size is about 6.4 million. The aircraft grid and the flow field grid are shown in Fig.8(a). The boundary conditions are given in Fig.8(b), in which the rear boundary of the aircraft is the pressure outlet boundary condition, and the rest are the velocity inlet boundary conditions.

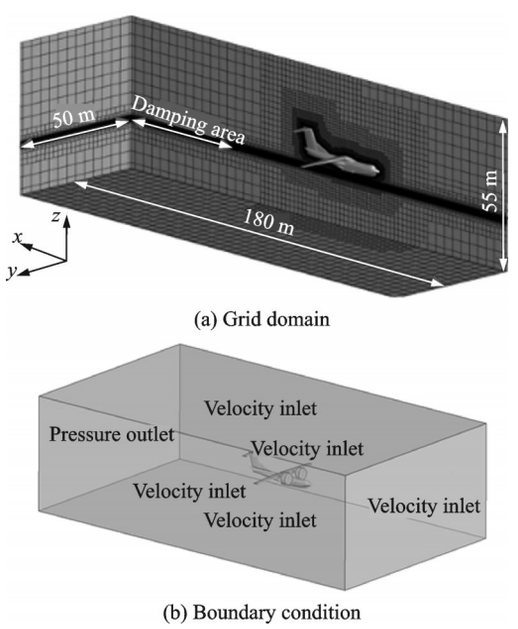

Fig.8 Grid domain and boundary condition

3.3 Results and analysis

In this section, the macroscopic aerodynamic characteristics of the seaplane are analyzed when the sideslip angle changes from 0° to 8° (an interval of 2°) in the ground effect area under the condition of wavy water surface.

Fig.9 shows the comparison between the aerodynamic forces, such as lift coefficient C_l, drag coefficient C_d, roll moment C_x, pitch moment and yaw moment coefficient C_y of the aircraft, and the coefficient C_z wave time history curve at the aerodynamic center position at different sideslip angles. It can be seen that when the sideslip angle varies in the range of 0° to 8°, the frequency of aerodynamic force change received by the aircraft is consistent with the frequency of wave encounter, and the change period of both is 0.6 s. With the increase of sideslip angle, the lift coefficient (Fig.9(a)) and pitching moment coefficient (Fig.9(d)) decrease, but the fluctuation amplitude hardly changes. The drag coefficient (Fig.9(b)) increases with the increase of sideslip angle, and the fluctuation amplitude does not show correlation. The rolling moment coefficient (Fig.9(c)) and yaw moment coefficient (Fig.9(e)) increase with the increase of sideslip angle, and the fluctuation amplitudes of them also increase significantly with the increase of sideslip angle. The fluctuation amplitude of rolling moment increases by 1.5 times and yaw moment increases by 2 times.

Fig.10 shows the curve of the mean aerody-

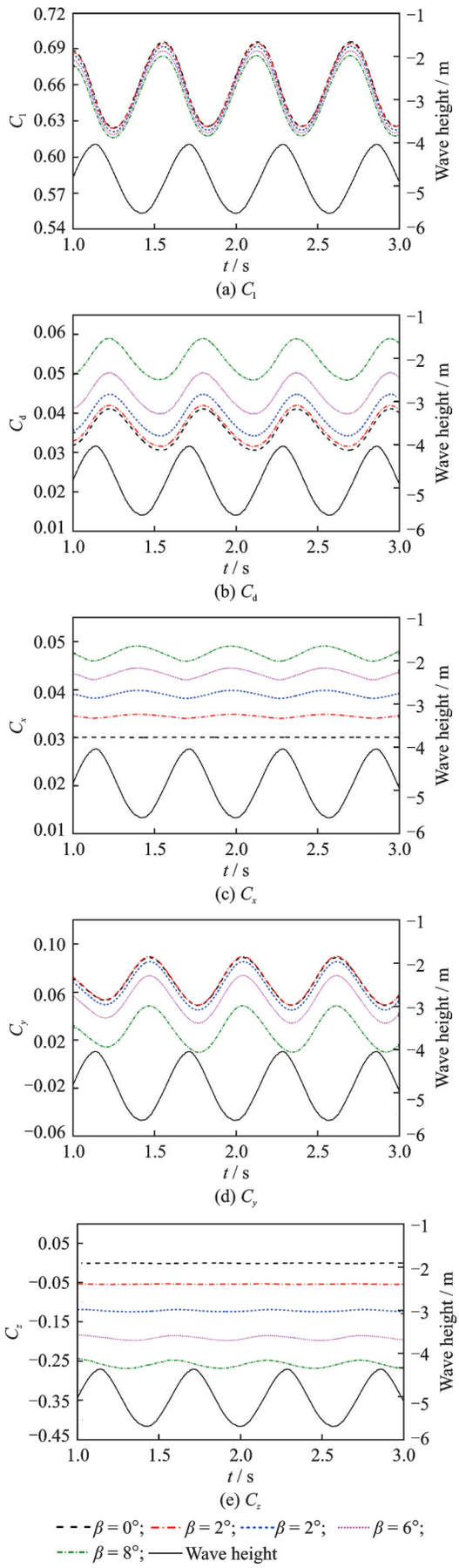

Fig.9 Fluctuation of aerodynamic coefficients at different sideslip angles

namic force of the aircraft changing with the sideslip angle. It can be seen that when the sideslip angle is small, the lift coefficient (Fig.10(a)) and the pitching moment coefficient (Fig.10(d)) do not change significantly. As shown in Fig.10(a) and Fig.10(d), when the sideslip angle changes from 0° to 4°, the mean lift coefficient decreases by about 0.045 and the pitching moment coefficient by about 0.004. When the sideslip angle is greater than 4°, the coefficient changes significantly with the increase of sideslip angle. The sideslip angle increases from 4° to 8°, the lift coefficient decreases by 0.065, and the pitching moment decreases by 0.036. Fig.10(b) shows the curve of the drag coefficient changing with the sideslip angle. It can be seen that the decrease of the drag coefficient also presents the same rule. When the sideslip angle changes from 0° to 4°, the mean drag coefficient increases by 0.003 5. When the sideslip angle increases from 4° to 8°, the mean drag coefficient increases by about 0.014. The curve of rolling moment coefficient(Fig.10(c)) and yaw moment coefficient(Fig.10(e)) changing with sideslip angle is different from the above law. When the sideslip angle is 0°, C_x and C_z are both 0. As the sideslip angle increases, both of them are almost lin-

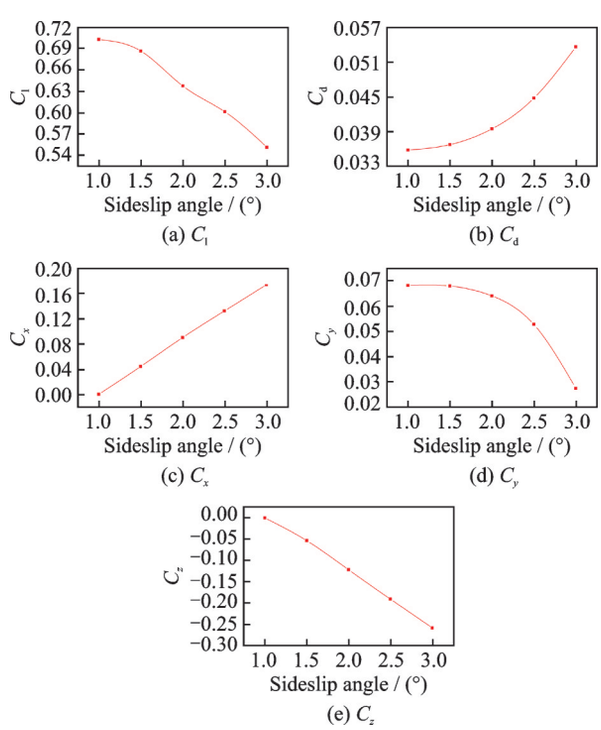

Fig.10 Mean aerodynamic coefficients at different sideslip angles

early related to the sideslip angle, with slopes of 0.022 and −0.032, respectively.

Fig.11(a) shows the cloud maps of aircraft surface pressure coefficient at different sideslip angles. It can be seen that when sideslip angle changes from 0° to 8°, the asymmetry of pressure coefficient distribution on both sides of the aircraft gradually becomes obvious, which is mainly reflected in the nose, vertical tail and horizontal tail. The pressure coefficient on the main wing does not change much with the sideslip angle. The decrease of the lift coefficient is mainly due to the increase of the sideslip angle, which leads to the change of the wing profile. However, the change range of the sideslip angle is not large. As shown in Fig.10(a), the decrease value of mean lift coefficient is about 0.01. As for the drag coefficient, due to the increase of sideslip angle, the incoming flow changes from the head-on flow at 0° sideslip to the fuselage at a certain angle, and the airflow directly impacts the fuselage, generating instability and greater drag. The result is an increase of about 0.028. The pitching moment coefficient is mainly related to the main wing and the horizontal tail. During the increase of sideslip angle, the aerodynamic characteristics of the horizontal tail change significantly, and the mean value of the pitching moment changes due to the decrease of lift coefficient. Fig.11(c) shows the pressure coefficient of horizontal tail during the change of sideslip angle. With the increase of sideslip angle, the negative pressure zone appears on the upper surface of the right horizontal tail and the lower surface of the left horizontal tail of the aircraft, which is most obvious when the sideslip angle is 8°. The uneven force on both sides leads to the increase of rolling moment of the aircraft. Fig.11(b) shows the distribution of the pressure coefficient of the aircraft vertical tail. The negative pressure area on the left vertical tail of the aircraft becomes more and more obvious, and correspondingly, the high pressure area on the right vertical tail becomes obvious. This is because the sideslip condition is equivalent to change the angle of attack of the vertical tail, causing the lateral force generated by the vertical tail to increase, and the absolute value of the aircraft's yaw moment increases.

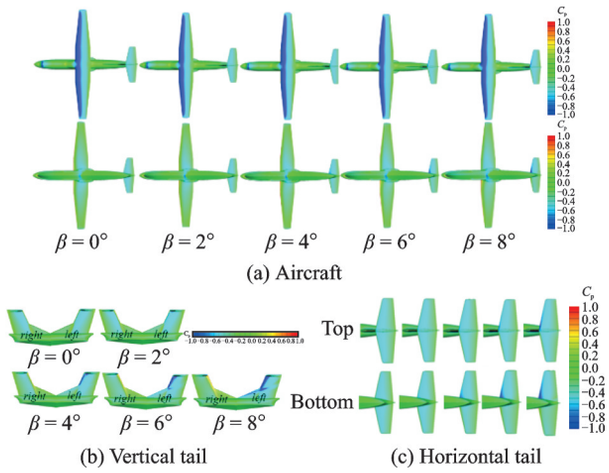

Fig.11 Cloud maps of pressure coefficient

However, since the direction of the yaw moment is along the negative direction of z-axis, the value of the moment is less than zero.

4 Conclusions

A numerical simulation of the flying process of a large seaplane above the wavy water surface is carried out. By changing the sideslip angle, the conclusions are obtained as follows:

(1) When the seaplane is flying above the linear wave surface, the aerodynamic force presents a periodic law, and the period of change is 0.6 s consistent with the wave period.

(2) As the sideslip angle increases, the average value of the lift coefficient and pitch moment coefficient decreases, the drag coefficient increases, and the fluctuation amplitude of the aerodynamic coefficient does not change.

(3) The mean value of the rolling moment coefficient and the mean absolute value of the yaw moment coefficient increase linearly with the sideslip angle, and their fluctuation amplitude also increases with the increase of the sideslip angle.

References

[1] JUNG K H, CHUN H H, KIM H J. Experimental investigation of wing-in-ground effect with a NACA6409 section[J]. Journal of Marine Science & Technology, 2008, 13(4): 317-327.

[2] AHMED M R, TAKASAKI T, KOHAMA Y. Aerodynamics of a NACA4412 airfoil in ground effect[J].AIAA Journal, 2012, 45(1): 37-47.

[3] HAN L, CHEN Y L, WANG F X. Numerical simu-

lation and aerodynamics analysis of Airfoil flying over wave ground at high grade sea condition[J]. Journal of Shanghai Jiaotong University, 2014, 48(8): 1127-1133. (in Chinese)

[4] QU Q L, LIU P Q, QIN X G. Numerical research on aerodynamic characteristics of WIG craft flying over wavy ground[J]. Acta Aeronautica et Astronautica Sinica, 2007, 28(6): 1327-1333.

[5] QIN X G, LIU P Q, QU Q L. Numerical simulation on aerodynamics of airfoil flying over wavy water surface[J]. Journal of Beijing University of Aeronautics and Astronautics, 2011, 37(3): 295-299, 304. (in Chinese)

[6] ZHI H L, XIAO T H, CHEN J C. Numerical analysis of aerodynamics of a NACA4412 airfoil above wavy water surface[C]//Proceedings of AIAA Aviation 2019 Forum.[S.l.]: AIAA, 2019: 3642.

[7] SHENG Q H, DE-MING W U, ZHANG L. Aerodynamic forces acting on an albatross flying above sea-waves[J]. Applied Mathematics and Mechanics, 2005, 26(9): 1222-1229.

[8] ZHONG M, HUA J, ZHENG S, et al. Propeller slipstream interference of large amphibian aircraft under take-off and landing configuration with crosswind[J]. Acta Aeronautica et Astronautica Sinica, 2018, 40(1): 125-135.

[9] LU Y J, XIAO T H, LI Z Z, et al. Numerical simulation of high speed plate ditching[J]. Acta Aeronautica et Astronautica Sinica, 2017, 38(S1): 6-14.

[10] JIN Y T, CHEN J C, LU Y J, et al. Numerical simulation of wedge impacting on wavy water[J]. Acta Aeronautica et Astronautica Sinica, 2019, 40(10): 46-59.

[11] BARBER T J. The free surface deformation caused by a wing in ground effect flying over water[C]//Proceedings of Pacific 2004 International Maritime Conference. Sydney: Pacific 2004 International Maritime Conference Managers, 2004.

Authors Mr. **LI Yanghui** received the B.S. degree and the M. S. degree in aircraft design from Nanjing University of Aeronautics and Astronautics in 2018 and 2021, respectively. His research interests include multi-phase flow and fluid-structure interaction.

Prof. **Tong Mingbo** received his Ph.D. degree in solid mechanics from Beijing University of Aeronautics of Astronautics in 1995. His research interest includes solid mechanics and aircraft design and analysis.

Author contributions Mr. **LI Yanghui** designed the study, complied the models, conducted the analysis, interpreted the results and wrote the manuscripts. Ms. **FU Xiaoqin** helped to research the background. Mr. **CHEN Jichang** and Prof. **TONG Mingbo** contributed to the discussion of the study. All authors commented on the manuscript draft and approved the submission.

Competing interests The authors declare no competing interests.

(Production Editor: SUN Jing)

水上飞机侧风波浪水面地面效应数值模拟

李阳辉，付晓琴，陈吉昌，童明波

（南京航空航天大学飞行器先进设计技术国防重点学科实验室，南京 210016，中国）

摘要：在绝对坐标系下，求解基于有限体积法的非定常雷诺平均Navier-Stokes（URANS）方程和k-ω SST湍流模型，模拟大型水上飞机在波面地效应区飞行时的气动特性。采用速度入口造波法和流体体积分数模型对线性规则波进行了精确模拟，并对自由表面进行了精确捕捉。本文主要研究了大型水上飞机在波浪水面上巡航时侧滑角对其气动特性的影响。结果表明：波浪水面地面效应主要影响机翼下表面的压力分布。当侧滑角在0°～8°范围内变化时，气动力的变化频率与波浪相遇频率一致，周期均为0.6 s。随着侧滑角的增大，升力系数和俯仰力矩系数均减小。然而，当侧滑角小于4°时，下降幅度较小，当侧滑角大于4°时，下降幅度显著，在整个侧滑角变化过程中，气动波动幅度几乎没有变化。阻力系数随侧滑角的增大而增大，当侧滑角大于4°时也出现显著增大阶段，且波动幅度不存在相关性。横摇力矩系数和横摆力矩系数均随侧滑角的增大而增大，其波动幅度均随侧滑角的增大而线性增大。

关键词：两相流；地面效应；流体体积分数模型；速度入口造波